Signal Processing 203 (2023) 108785

Contents lists available at ScienceDirect

Signal Processing

journal homepage: www.elsevier.com/locate/sigpro

Order-Statistic Based Target Detection with Compressive Measurements in Single-Frequency Multistatic Passive Radar☆

Junhu Ma[a,b,c], Hongbin Li[b], Lu Gan[a,*]

[a] School of Information and Communication Engineering, University of Electronic Science and Technology of China, Chengdu, Sichuan 611731, China
[b] Department of Electrical and Computer Engineering, Stevens Institute of Technology, Hoboken, NJ 07030, USA
[c] Southwest China Institute of Electronic Technology, Chengdu, Sichuan 610036, China

ARTICLE INFO

Article history:
Received 27 September 2021
Revised 23 August 2022
Accepted 16 September 2022
Available online 20 September 2022

Keywords:
Multistatic passive radar
Single-frequency network
Compressive target detection
Order-statistic
Orthogonal matching pursuit

ABSTRACT

This paper considers the problem of compressive target detection with direct-path interference (DPI) and clutter in a single-frequency network (SFN) based multistatic passive radar system (MS-PRS). Specifically, a measurement matrix is designed to jointly obtain compressive observations and remove the DPI and clutter. We first analyze a compressive subspace detector which assumes the target support is known. When the target supports cannot be accurately obtained, an order-statistic (OS) based detector, referred to as the OSOMP, is proposed by using the orthogonal matching pursuit (OMP) algorithm to estimate the target support, and then projecting the compressive observations into the estimated subspace. Since OMP applies an iterative ranking process to select the components/atoms of the dictionary, the OSOMP test variable is an order statistic, which has a non-convergent distribution. To cope with this problem, a modified test statistic for the OSOMP detector is presented and an analytical expression for the probability of false alarm is obtained. We further discuss the minimum number of iterations required by the OSOMP algorithm to achieve the desired probability of detection and false alarm. Numerical simulations are conducted to verify the theoretical analysis and illustrate the performance of the proposed detector relative to several benchmark detectors.

© 2022 Elsevier B.V. All rights reserved.

1. Introduction

Passive radar (PR) exploiting non-cooperative illuminators of opportunity (IOs) has been an active topic of interest over the past decades [1]. In contrast to a conventional active radar, the PR has the advantages of low cost, covertness, and availability of diverse IO sources, such as frequency modulation (FM) radio, digital audio broadcasting (DAB), digital video broadcasting-terrestrial (DVB-T), mobile communication networks, and others. There are two broadly defined PR systems, namely bistatic PR system and multistatic PR system (MS-PRS). In recent years, MS-PRS has been widely investigated for practical civilian and military applications, because it offers some unique sensing opportunities compared with its bistatic counterpart [2–4]. Meanwhile, since the target echo is sparse in the delay-Doppler domain, compressive sensing (CS), an emerging technique which helps reduce the computational and data-collection related burden, has attracted much attention in radar signal processing [5]. This paper considers the problem of target detection by using a CS-based framework in MS-PRS comprising multiple IOs and one receiver, where the IOs are from a single-frequency network (SFN) that transmits a common signal [6].

The target detection problem is equivalent to determining the presence/absence of the target of interest [7,8]. However, a major challenge associated with target detection in MS-PRS is the removal of the direct-path interference (DPI) and clutter [9–11]. A number of methods have been introduced to address the problem, including an adaptive beamforming (AB) technique [9], a least mean square (LMS) method [10], and an extensive cancellation algorithm (ECA) [11], among others. The AB method has limited interference rejection ability when the size of array aperture is small, while the LMS method converges slowly and has a high computational complexity [12]. The ECA, which projects the received surveillance signals into a subspace orthogonal to the DPI and clutter subspace, is a popular choice for DPI/clutter rejection due to its flexibility.

☆ This work was partly completed during the first author's visit to the Stevens Institute of Technology, Hoboken, NJ 07030, USA. The work of H. Li was supported in part by the National Science Foundation under Grants ECCS-1923739 and ECCS-2212940. The work of L. Gan was supported in part by Yibin Scienceand Technology Program under Grant 2020FW007 and YBP-002.

* Corresponding author.
E-mail addresses: mjh_uestc@126.com (J. Ma), hli@stevens.edu (H. Li), ganlu@uestc.edu.cn (L. Gan).

https://doi.org/10.1016/j.sigpro.2022.108785
0165-1684/© 2022 Elsevier B.V. All rights reserved.

For target detection, MS-PRS can be divided into two categories depending on whether reference channels (RCs) are present or not [6,13–16]. In the absence of RCs, the generalized canonical correlation (GCC) detector, which assumes the noise variance is known, is proposed for target detection in MS-PRS with a single IO and multiple receivers [13]. The case of unknown noise variance is addressed in [14]. With the development of digital communication technique, the IOs may be overlapping or occupy the same transmit frequency band. Thus, SFN-based MS-PRS has been widely studied for target detection, location, and tracking[6,15,17]. Specifically, an SFN-based MS-PRS consisting of multiple IOs which transmit a common signal and one receiver is studied in [6], where the GCC detector is extended to this system for passive detection. On the other hand, in the presence of RCs, [15] considers target detection for an SFN-based MS-PRS when the single receiver is equipped with a large number of antennas. In the case of multiple IOs and multiple receivers, a linear fusion based passive multistatic target detection method is proposed in [16], where local test statistics are weighted by an optimized set of weights at the fusion center. All above detection algorithms assume accurate knowledge of the positions of the receivers and the IOs. Due to the non-cooperative nature of IOs, the location information may be inaccurately obtained. Although the energy detector (ED) [14] does not require the location information, it is sensitive to the noise level [18].

Recently, considering that the target echo is sparse in the delay-Doppler domain, CS-based radar signal processing has attracted much attention to overcome the resolution problems and relieve the burden of hardware cost [19–25]. While most of such efforts are devoted to reconstructing the compressive signal first and then using the reconstructed signal for detection/estimation. It is worth noting that the purpose of target detection is to determine the presence/absence of the target of interest, there is no need to reconstruct the original signal, which would result in additional computations. In addition, it is well-known that the reconstruction algorithms are sensitive to noise and require high SNRs. It has been proved in [26] that the power loss is only caused by data compression, and there is almost no power loss when integrating signal in the compressed domain. Therefore, there is an interest in direct compressive detection of a sparse signal without reconstruction, which can further reduce the complexity [26–30]. One piece of work that is closely related the current paper is [30], which first discusses how to determine the minimum fraction of the target support to achieve a desired detection performance when the support is known. Then, two distributed algorithms are presented for the case of unknown support by using the orthogonal matching pursuit (OMP) algorithm [31] to estimate the support. Assuming the support is correctly recovered, the above distributed detectors and analytical results are applied with the OMP-based support estimate. However, the OMP employs an iterative process to select the components/atoms of the dictionary that have the largest cross correlation with the observed signal. The selection process leads to an order statistic that affects the distribution of the decision variable, which is not considered in [30]. Besides, the methods of [30] cannot be directly applied for detection in MS-PRS, since the received target echoes have strong DPI and clutter.

In this paper, we consider the compressive target detection with DPI and clutter in an SFN-based MS-PRS. This system consists of multiple IOs transmitting a common signal and one receiver, where the receiver has an RC and a surveillance channel (SC). Different from the above detectors [6,13–16], we consider a case of where the locations of IOs are subject to positioning errors. Firstly, the dictionary matrix is built from the received reference signal, and a random measurement matrix is designed to jointly obtain compressive observations and remove the DPI and clutter in the received surveillance signals. Secondly, a complex-valued based compressive subspace detector (CSD) is briefly discussed under the assumption that the support of the target is known. For the case of unknown target support, that is, the positions of the IOs are not precisely known, an order-statistic based orthogonal matching pursuit (OSOMP) detector is proposed by integrating support estimation with target detection. Similar to the CSD, the test statistic of the OSOMP detector is obtained by projecting the compressive measurements into the estimated subspace. However, the OMP leads to an order statistic that is not convergent in distribution. To address the problem, a modified test statistic for the OSOMP detector is proposed. Besides, we also discuss the extension of the OSOMP detector for multi-target detection. A performance analysis is presented, which results in an analytical expression for the probability of false alarm of the OSOMP detector. To further reduce the computational complexity, we discuss the minimum number of iterations required by the OSOMP algorithm to achieve the desired probability of detection and false alarm, which can also cope with the case of an unknown number of IOs. Finally, numerical simulation results are presented to verify theoretical analysis and demonstrate the performance of the proposed detector. It is found that the OSOMP detector outperforms the ED in low and moderate signal-to-noise ratio (SNR) regions.

The rest of this paper is organized as follows. In Section 2, the signal model for the considered problem is introduced. Section 3 contains the derivation of the OSOMP detector. Performance analysis is given in Section 4. Numerical results are presented in Section 5, followed by conclusions in Section 6.

Notation: Vectors/Matrices are denoted by boldface lower/upper case letters. $(\cdot)^T$ and $(\cdot)^H$ represents the transpose and the complex conjugate transpose. The symbols $\sim$ and $\in$ mean "is distributed as" and "belongs to", respectively. $\mathcal{CN}\left(\mu,\sigma^2\right)$ represents a complex Gaussian distribution with mean μ and variance σ^2, $\mathrm{Exp}(\beta)$ denotes an exponential distribution with parameter β, $\Gamma(x)$ is the Gamma function, χ_N^2 represents the central Chi-squared distribution with N degrees of freedom, and $\chi_N^2(\lambda)$ represents the non-central Chi-squared distribution with non-centrality parameter λ. $\mathbf{I}_N$ is an N-dimensional identity matrix. $|\cdot|$ denotes the absolute value, $\|\cdot\|_2$ denotes the Frobenius norm, and $j=\sqrt{-1}$. For a matrix $\mathbf{A}$, $\mathbf{P}_{\mathbf{A}}=\mathbf{A}(\mathbf{A}^H\mathbf{A})^{-1}\mathbf{A}^H$, $\mathrm{rank}(\mathbf{A})$ denotes the rank of $\mathbf{A}$, and $\mathbf{A}(\boldsymbol{\mu})$ represents the columns of $\mathbf{A}$ indexed by $\boldsymbol{\mu}$.

2. Signal Model

2.1. Sparse Representation of Moving Target Echoes

As shown in Fig. 1, we consider an MS-PRS consisting of K non-cooperative IOs, which are a part of a single-frequency network transmitting a common signal, and one receiver [6]. The receiver is equipped with a RC and a SC. The RC, which is used to receive a copy of the IO source signal, can be formed by pointing an antenna to one of the K IOs. In the SC, the baseband-equivalent received signal includes a mixture of the direct-path, multi-path clutter interference, and target echo can be expressed as

$$y_{\mathrm{sc}}(n)=\sum_{l=1}^{L}\beta_l s(n-c_l)+\sum_{k=1}^{K}\alpha_k s(n-\tau_k)e^{j\Omega_{dk}n}+w(n),\quad n=1,\ldots,N, \tag{1}$$

where $s(n)$ denotes the transmitted signal, β_l denotes the complex amplitude of the direct path or clutter interference, c_l denotes the direct-path or multi-path time delay, α_k denotes the complex amplitude of the target echo, τ_k and Ω_{dk} denote the time delay and normalized Doppler shift of the target received by the k-th IO, respectively, and $w(n)$ denotes the Gaussian noise following $w(n)\sim\mathcal{CN}\left(0,\sigma^2\right)$. In this paper, we consider the case where the source signal $s(n)$ has been obtained from the reference channel observations by using IO some signal reconstruction technique (e.g., [32]).

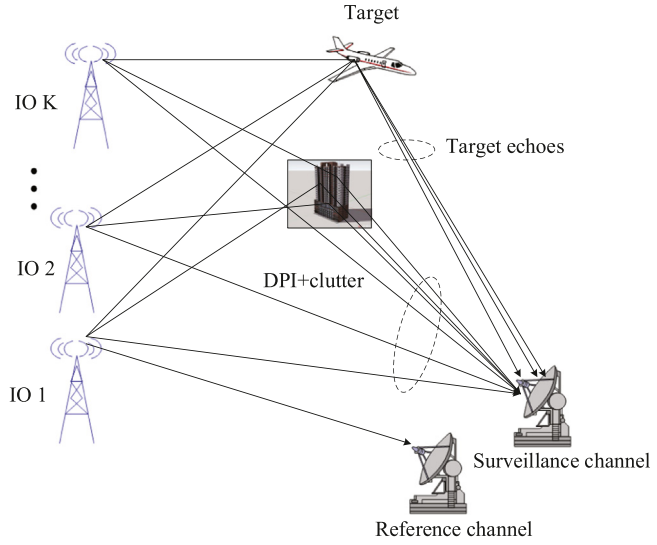

Fig. 1. A single-frequency network based multistatic passive radar system.

To facilitate discussion, the vector model of (1) can be written as

$$\mathbf{y}_{\mathrm{sc}} = \mathbf{s}_{\mathrm{c}} + \mathbf{s}_{\mathrm{e}} + \mathbf{w}_{\mathrm{sc}}, \tag{2}$$

where $\mathbf{y}_{\mathrm{sc}}$ is the $N \times 1$ SC observation vector, $\mathbf{s}_{\mathrm{c}}$, $\mathbf{s}_{\mathrm{e}}$, and $\mathbf{w}_{\mathrm{sc}}$ represent the interferences, observations of the moving target echoes, and the Gaussian noise, respectively, with

$$\mathbf{s}_{\mathrm{c}} = \left[\sum_{l=1}^{L}\beta_l s(1-c_l),\ \ldots,\ \sum_{l=1}^{L}\beta_l s(N-c_l)\right]^T, \tag{3}$$

$$\mathbf{s}_{\mathrm{e}} = \left[\sum_{k=1}^{K}\alpha_k s(1-\tau_k)e^{j\Omega_{dk}},\ldots,\sum_{k=1}^{K}\alpha_k s(N-\tau_k)e^{j\Omega_{dk}N}\right]^T, \tag{4}$$

$$\mathbf{w}_{\mathrm{sc}} = [w(1),\ \ldots,\ w(N)]^T. \tag{5}$$

It is well-known that the moving target echo $\mathbf{s}_e$ lies in the range-Doppler domain and has a sparse representation (e.g., [24])

$$\mathbf{s}_{\mathrm{e}} = \boldsymbol{\Psi}\boldsymbol{\alpha}, \tag{6}$$

where $\boldsymbol{\alpha} \in \mathbb{C}^{N\times 1}$ is the sparse vector with K non-zero elements, and $\boldsymbol{\Psi} \in \mathbb{C}^{N\times N}$ represents a dictionary matrix consisting of delay-and-Doppler-shifted copies of the reference signal $s(n)$ [11],

$$\boldsymbol{\Psi} = \mathbf{B}[\boldsymbol{\Lambda}_{-P}\mathbf{S},\ \cdots,\ \boldsymbol{\Lambda}_{-1}\mathbf{S},\ \mathbf{S},\ \boldsymbol{\Lambda}_{1}\mathbf{S},\ \cdots,\ \boldsymbol{\Lambda}_{P}\mathbf{S}], \tag{7}$$

where $\mathbf{B} \in \{0,1\}^{N\times(N+Q)}$ is a selection matrix which selects the last N rows of its successor and is given by

$$\mathbf{B} = \{b_{uv}\}_{u=1,\cdots,N,v=1,\cdots,N+Q},\quad b_{uv} = \begin{cases}1, & u = v-Q,\\ 0, & \text{otherwise},\end{cases} \tag{8}$$

with Q representing the number of time delay cells. $\boldsymbol{\Lambda}_p \in \mathbb{C}^{(N+Q)\times(N+Q)}$ denotes a Doppler shift operator corresponding to the p-th Doppler bin, which is a diagonal matrix

$$\boldsymbol{\Lambda}_p = \begin{bmatrix}1 & 0 & \cdots & 0\\ 0 & e^{j\Omega_p 2} & \cdots & 0\\ \vdots & \vdots & \ddots & \vdots\\ 0 & 0 & \cdots & e^{j\Omega_p(N+Q-1)}\end{bmatrix},\ p = -P,\cdots,0,1,\cdots,P, \tag{9}$$

where Ω_p is the normalized Doppler shift of the p-th Doppler bin satisfying $\Omega_p = \frac{2\pi pB_{\mathrm{D}}}{(2P+1)f_s}$ with B_{D} representing the Doppler bandwidth in Hz, and f_s denoting the sampling frequency. $\mathbf{S} \in \mathbb{C}^{(N+Q)\times Q}$ is given by

$$\mathbf{S} = [\mathbf{s},\ \mathbf{Ds},\ \cdots,\ \mathbf{D}^{(Q-1)}\mathbf{s}], \tag{10}$$

where $\mathbf{s} \in \mathbb{C}^{(N+Q)\times 1}$, and

$$\mathbf{s} = [s(-Q+1),\ \cdots,\ s(0),\cdots s(N)]^T. \tag{11}$$

To ensure the signal is fully integrated, $N+Q$ samples of $s(n)$ are collected [11]. Besides, $\mathbf{D} \in \mathbb{R}^{(N+Q)\times(N+Q)}$ denotes a delay matrix which is given by

$$\mathbf{D} = \{d_{uv}\}_{u,v=1,\cdots,N+Q},\quad d_{uv} = \begin{cases}1, & u = v+1,\\ 0, & \text{otherwise}.\end{cases} \tag{12}$$

Without the loss of generality, assume that $N = Q(2P+1)$, and thus we have $\boldsymbol{\Psi} \in \mathbb{C}^{N\times N}$.

2.2. Compressive Detection with Interference Cancellation

Based on the CS theory, a sparse signal can be recovered from fewer measurements with sub-Nyquist sampling to reduce the burden of computation and data collection. In this paper, the problem of interest is to consider a moving target detection problem by using compressive observations:

$$\begin{cases}H_0 : \bar{\mathbf{y}} = \bar{\boldsymbol{\Phi}}\mathbf{s}_{\mathrm{c}} + \bar{\mathbf{w}},\\ H_1 : \bar{\mathbf{y}} = \bar{\boldsymbol{\Phi}}\mathbf{s}_{\mathrm{c}} + \bar{\boldsymbol{\Phi}}\boldsymbol{\Psi}\boldsymbol{\alpha} + \bar{\mathbf{w}},\end{cases} \tag{13}$$

where $\bar{\mathbf{y}} = \bar{\boldsymbol{\Phi}}\mathbf{y}_{\mathrm{sc}}$, $\bar{\boldsymbol{\Phi}} \in \mathbb{R}^{M\times N}$ $(K \ll M \ll N)$ satisfying the restricted isometry property (RIP) represents a compressive random measurement matrix, and $\bar{\mathbf{w}} = \bar{\boldsymbol{\Phi}}\mathbf{w}_{\mathrm{sc}}$.

In order to expose weak target, interference cancellation must be carried out prior to target detection. Suppose that the direct-path or clutter interferences $\mathbf{s}_{\mathrm{c}}$ are considered backscattered from the first L range cells with zero Doppler shifts [11], i.e., it can be expressed as

$$\mathbf{s}_{\mathrm{c}} = \boldsymbol{\Psi}_{\mathrm{c}}\boldsymbol{\beta}, \tag{14}$$

where $\boldsymbol{\Psi}_{\mathrm{c}} \in \mathbb{C}^{N\times L}$ is a submatrix of $\boldsymbol{\Psi}$ which spans the subspace of $\mathbf{s}_{\mathrm{c}}$, and $\boldsymbol{\beta} \in \mathbb{C}^{L\times 1}$ denotes the subspace coefficients. Thus, the DPI and clutter can be removed by using the ECA [11]. Inspired by the ECA, we design the measurement matrix as

$$\boldsymbol{\Phi} = \bar{\boldsymbol{\Phi}}\mathbf{P}^{\perp}_{\boldsymbol{\Psi}_{\mathrm{c}}}. \tag{15}$$

where

$$\mathbf{P}^{\perp}_{\boldsymbol{\Psi}_{\mathrm{c}}} = \mathbf{I}_N - \boldsymbol{\Psi}_{\mathrm{c}}\left(\boldsymbol{\Psi}_{\mathrm{c}}^H\boldsymbol{\Psi}_{\mathrm{c}}\right)^{-1}\boldsymbol{\Psi}_{\mathrm{c}}^H. \tag{16}$$

Then, replacing $\bar{\boldsymbol{\Phi}}$ with $\boldsymbol{\Phi}$ in (13) yields

$$\begin{cases}H_0 : \mathbf{y} = \mathbf{w},\\ H_1 : \mathbf{y} = \boldsymbol{\Theta}\boldsymbol{\alpha} + \mathbf{w},\end{cases} \tag{17}$$

where $\boldsymbol{\Theta} = \boldsymbol{\Phi}\boldsymbol{\Psi}$ denotes the sensing matrix and $\mathbf{w} = \boldsymbol{\Phi}\mathbf{w}_{\mathrm{sc}}$. It is clear $\mathbf{w} \sim \mathcal{CN}\left(\mathbf{0}, \sigma^2\boldsymbol{\Phi}\boldsymbol{\Phi}^H\right)$. In practice, the dimension of clutter is usually far less than the measured samples, i.e., we can assume that $L \ll M \ll N$ and $N - L > M$. Then, $\mathrm{rank}\left(\boldsymbol{\Phi}\boldsymbol{\Phi}^H\right) = M$, which is shown in Appendix A.

3. Target Detection

In this section, we first briefly discuss the CSD that assumes the support of the target is known. However, in a MS-PRS, the support of the target echo may not be exactly known due to the non-cooperative nature of the IOs. To address this problem, we propose an OSOMP detector which integrates support estimation in target detection.

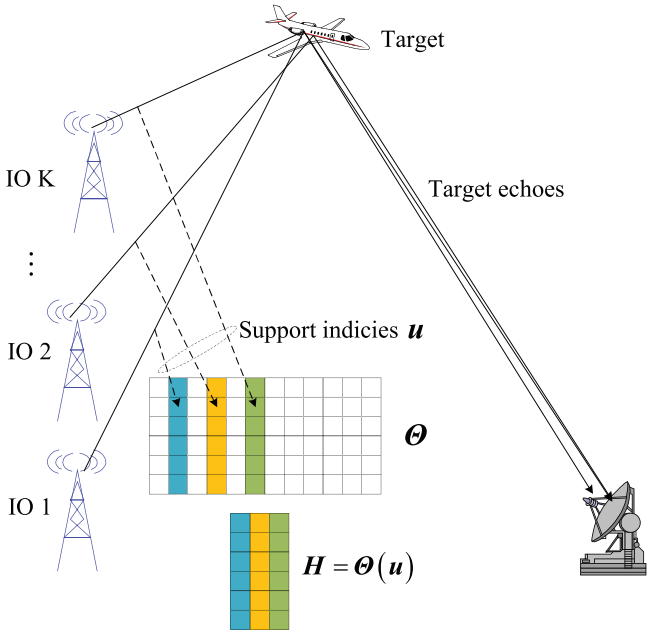

Fig. 2. Compressive subspace detector with known locations on IOs.

3.1. CSD with Known Target Support

As shown in Fig. 2, suppose that there are K IOs and one target in an SFN-based MSPR system. When the locations of these IOs are exactly known, the support set indices $\mathbf{u}$ of the target can be obtained [6], where $\mathbf{u} := \{i \in \{1, \cdots, N\} | \boldsymbol{\alpha}(i) \neq 0\}$, and $\boldsymbol{\alpha}(i)$ represents the i-th element of $\boldsymbol{\alpha}$. Then, the detection problem of (17) can be rewritten as

$$\begin{cases} H_0 : \mathbf{y} = \mathbf{w}, \\ H_1 : \mathbf{y} = \mathbf{H}\tilde{\boldsymbol{\alpha}} + \mathbf{w}, \end{cases} \tag{18}$$

where $\mathbf{H} = \boldsymbol{\Theta}(\mathbf{u})$ represents the target support matrix, which is an $M \times K$ submatrix of the sensing matrix $\boldsymbol{\Theta}$ with columns indexed by $\mathbf{u}$, and $\tilde{\boldsymbol{\alpha}} \in \mathbb{C}^{K\times 1}$ denotes the K nonzero elements of $\boldsymbol{\alpha}$. According to [30], the test statistic of the complex-valued based CSD is given by

$$T_{\text{CSD}} = \frac{\left\| \mathbf{P}_{\mathbf{H}} \left(\boldsymbol{\Phi}\boldsymbol{\Phi}^H \right)^{-\frac{1}{2}} \mathbf{y} \right\|_2^2}{\sigma^2/2}, \tag{19}$$

where $\mathbf{P}_{\mathbf{H}} = \mathbf{H}(\mathbf{H}^H\mathbf{H})^{-1}\mathbf{H}^H$, and $\left(\boldsymbol{\Phi}\boldsymbol{\Phi}^H\right)^{-\frac{1}{2}}$ denotes the whitening operator. Under the assumption that the support is known, the distribution of T_{CSD} is given by

$$\begin{cases} H_0 : T_{\text{CSD}} \sim \chi^2_{2K}, \\ H_1 : T_{\text{CSD}} \sim \chi^2_{2K}(\lambda_{\text{CSD}}), \end{cases} \tag{20}$$

where $\lambda_{\text{CSD}} = \frac{\left\| \mathbf{P}_{\mathbf{H}} (\boldsymbol{\Phi}\boldsymbol{\Phi}^H)^{-\frac{1}{2}} \mathbf{H}\tilde{\boldsymbol{\alpha}} \right\|_2^2}{\sigma^2/2}$. The performance of the CSD is derived in Appendix B.

Nevertheless, when the target support $\mathbf{H}$ is unknown, which may occur in practical MS-PRS, the CSD becomes unusable. Next, we propose an OSOMP detector by jointly detecting and estimating the target support $\mathbf{H}$.

3.2. Proposed OSOMP Detector with Unknown Target Support

In conventional MS-PRS detection, the geographical locations of the IOs and the receiver are often assumed known exactly, so that the relative target delays τ_k and Doppler shifts f_k, $k = 1, \ldots, K$, among the received target echoes can be compensated first, and then the detectors in [6,13,14] are proposed for target detection. However, the location of IOs may not be measured accurately in practical PR scenario, i.e. the target support may not be precisely known. Therefore, there is a need for an improved solution to cope with such uncertainty by jointly estimating the subspace matrix $\mathbf{H}$ and performing target detection. To facilitate discussion, we first consider the situation where there is a single target in the surveillance area.

Specifically, when the target subspace $\mathbf{H}$ is imprecisely known, we can obtain an estimate $\hat{\mathbf{H}}$ by using a sparsity recovering technique, such as the OMP algorithm [31]. Similar to the CSD, the test statistic of the OSOMP detector can be expressed as

$$\bar{T}_{\text{OSOMP}} = \frac{\sum_{k=1}^{K} \left\| \mathbf{P}_{\boldsymbol{\Theta}(\mu_k)} \left(\boldsymbol{\Phi}\boldsymbol{\Phi}^H \right)^{-\frac{1}{2}} \mathbf{y} \right\|_2^2}{\sigma^2/2}, \tag{21}$$

where $\boldsymbol{\Theta}(\mu_k) \in \mathbb{C}^{M\times 1}$ represents the μ_k-th column of $\boldsymbol{\Theta}$, $\mathbf{P}_{\boldsymbol{\Theta}(\mu_k)} = \boldsymbol{\Theta}(\mu_k)\left(\boldsymbol{\Theta}(\mu_k)^H\boldsymbol{\Theta}(\mu_k)\right)^{-1}\boldsymbol{\Theta}(\mu_k)^H$, μ_k denoting the index of the k-th iteration is given by

$$\mu_k = \arg \max_{i\in\{1,\ldots,N\}} |< \mathbf{r}_{k-1}, \boldsymbol{\Theta}(i) >|, \quad k = 1, \ldots, K, \tag{22}$$

$\mathbf{r}_k$ representing the residual vector at the k-th iteration of the OMP algorithm is

$$\mathbf{r}_k = \left(\mathbf{I}_N - \mathbf{P}_{\boldsymbol{\Theta}(\mu_k)}\right)\mathbf{y}, \tag{23}$$

with $\mathbf{r}_0 = \mathbf{y}$, and the support set is formed by

$$\boldsymbol{\mu}_k = \boldsymbol{\mu}_{k-1} \cup \{\mu_k\}, \tag{24}$$

with $\boldsymbol{\mu}_0 = \emptyset$. Eq. (22) shows that the index μ_k is obtained by finding the most correlated column between the sensing matrix $\boldsymbol{\Theta}$ and the residual vector.

Correspondingly, let

$$t_i = \frac{\left\| \mathbf{P}_{\boldsymbol{\Theta}(i)} (\boldsymbol{\Phi}\boldsymbol{\Phi}^H)^{-\frac{1}{2}} \mathbf{y} \right\|_2^2}{\sigma^2/2}, \qquad i = 1, \ldots, N, \tag{25}$$

which are used to form a set

$$\mathcal{T} = \{t_1, \cdots, t_N\}. \tag{26}$$

From (21)-(25), we can see

$$\frac{\left\| \mathbf{P}_{\boldsymbol{\Theta}(\mu_k)} (\boldsymbol{\Phi}\boldsymbol{\Phi}^H)^{-\frac{1}{2}} \mathbf{y} \right\|_2^2}{\sigma^2/2} \in \mathcal{T}, \tag{27}$$

or more precisely, $\frac{\left\| \mathbf{P}_{\boldsymbol{\Theta}(\mu_k)} \left(\boldsymbol{\Phi}\boldsymbol{\Phi}^H\right)^{-\frac{1}{2}} \mathbf{y} \right\|_2^2}{\sigma^2/2}$ represents the k-th largest element of $\mathcal{T}$. Then, we denote

$$t_{(N-k+1)} = \frac{\left\| \mathbf{P}_{\boldsymbol{\Theta}(\mu_k)} (\boldsymbol{\Phi}\boldsymbol{\Phi}^H)^{-\frac{1}{2}} \mathbf{y} \right\|_2^2}{\sigma^2/2}, \qquad k = 1, \ldots, K, \tag{28}$$

where $t_{(i)}$ represents the order statistic of t_i with

$$t_{(1)} \leq \cdots \leq t_{(i)} \leq \cdots \leq t_{(N)}. \tag{29}$$

Substituting (28) into (21), we can write the test statistic of the OSOMP detector as

$$\bar{T}_{\text{OSOMP}} = \sum_{k=1}^{K} t_{(N-k+1)}. \tag{30}$$

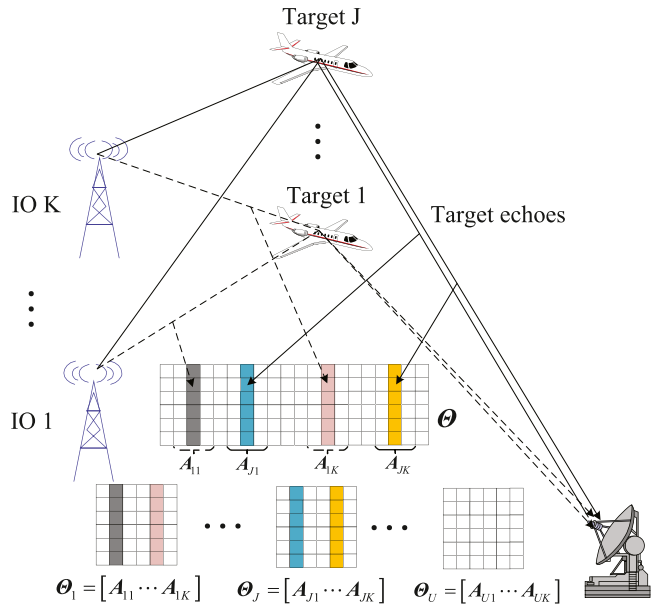

Fig. 3. OSOMP detector for multiple targets, where $\mathbf{\Theta}_1$ contains the possible subspace of target 1, and $\mathbf{\Theta}_J$ contains the possible subspace of target J.

3.3. An Equivalent Form of the OSOMP Detector

It turns out the distribution of $\bar{T}_{\text{OSOMP}}$ is not convergent in the following analysis, which necessitates an alternative form for implementation.

Specifically, according to (20), it can be easily shown that the distribution of t_i in (25) under the H_0 hypothesis is

$$t_i \sim \chi_2^2, \qquad \text{under } H_0. \tag{31}$$

Note that t_i is also an exponential distribution with $t_i \sim \text{Exp}\left(\frac{1}{2}\right)$ and its cumulative distribution function (CDF) is

$$F_{t_i}(t) = 1 - e^{-\frac{t}{2}}. \tag{32}$$

It follows from (31) and (32) that $\bar{T}_{\text{OSOMP}}$ under H_0 is the trimmed sums of the first K largest values of the order statistic of the exponential distribution. However, the distribution of $\bar{T}_{\text{OSOMP}}$ is non-convergent in the case of $K \geq 2$ and large N [33]. To address this problem, a modified and alternative form T_{OSOMP} that is equivalent to $\bar{T}_{\text{OSOMP}}$ but with a convergent CDF is given by

$$T_{\text{OSOMP}} = \bar{T}_{\text{OSOMP}} - 2K\log(N). \tag{33}$$

Therefore, we can replace $\bar{T}_{\text{OSOMP}}$ with T_{OSOMP} in the following derivation, and the OSOMP detector can be equivalently expressed as

$$T_{\text{OSOMP}} \underset{H_0}{\overset{H_1}{\gtrless}} \eta, \tag{34}$$

where η denotes the detection threshold. The implementation of the OSOMP detector is summarized in Algorithm 1.

3.4. OSOMP for Multiple Targets

In this subsection, we discuss the extension of the OSOMP detector for multi-target detection. As shown in Fig. 3, which depicts a case with J targets in the surveillance area, where the number of targets J is unknown. In an MS-PRS, K IOs jointly monitor targets that may exist in the surveillance area. When detecting the target of interest, it is standard to divide the surveillance area into different detection cells in the delay-Doppler domain, and the super dictionary matrix $\mathbf{\Psi}$ consisting of delay-and-Doppler-shifted copies of the reference signal covers all detection cells. Suppose that the possible signal subspaces of target 1 corresponding to IO 1 to IO K are $\mathbf{A}_{11}, \cdots, \mathbf{A}_{1K}$, respectively. Therefore, the sensing matrix of target 1 is denoted as $\mathbf{\Theta}_1 = [\mathbf{A}_{11}, \cdots, \mathbf{A}_{1K}]$. Correspondingly, the sensing matrix of target J is given by $\mathbf{\Theta}_J = \left[\mathbf{A}_{J1}, \cdots, \mathbf{A}_{JK}\right]$, where $\mathbf{A}_{Jk}$ represents the possible signal subspace of target J corresponding to IO k. For well separated targets, it is reasonable to assume that the dictionaries are non-overlapping, i.e., $\mathbf{\Theta}_i \cap \mathbf{\Theta}_j = \emptyset$, where $i \neq j, i, j \in \{1, \cdots, J\}$. This is equivalent to the assumption that, in conventional radar systems, different targets located in different resolution cells are associated with different ranges and Doppler frequencies. As illustrated in Fig. 3, the super sensing matrix $\mathbf{\Theta}$ subsumes individual sensing matrices for all J targets. Therefore, the multi-target detection problem can be solved by Algorithm 1 by using the super sensing matrix $\mathbf{\Theta}$. In this case, the indices recovered by the OMP provide the support for all J targets. Finally, the passive radar will not be able to resolve closely spaced targets which, similarly as in conventional radar, will be treated as a single composite target that can be detected by our method.

4. Performance Analysis

In this section, we examine the performance of the proposed OSOMP detector. Due to the inherent sorting incurred by OMP, the OSOMP decision variable is an order statistic. We derive an expression of the order static under the H_0 hypothesis, which can be used to set the detection threshold and determine the false alarm probability P_{FA} for OSOMP. Under the H_1 hypothesis, since the support estimate obtained by OMP may consist of true target support and wrong support (from the noise subspace), especially at low SNR, an order-statistic based analysis becomes intractable. Hence, we resort to numerical approaches to determine the probability of detection for OSOMP detector in Section 5.

4.1. Probability of False alarm of OSOMP Detector

To derive the probability of false alarm of the proposed OSOMP detector, we consider the distribution of T_{OSOMP} (under the H_0 hypothesis) for two different cases with $K = 1$ and $K \geq 2$. Specifically, when $K = 1$, we have

$$T_{\text{OSOMP}} = t_{(N)} - 2\log(N). \tag{35}$$

From (31) and (32), the CDF $F_{T_{\text{OSOMP}}}(t)$ in (35) can be expressed as

$$\begin{aligned} F_{T_{\text{OSOMP}}}(t) &= P(T_{\text{OSOMP}} \leq t) \\ &= P\left(t_{(N)} \leq t + 2\log(N)\right) \\ &= P(\max(t_i) \leq t + 2\log(N)) \\ &= [F_{t_i}(t + 2\log(N))]^N \\ &= \left(1 - e^{-\frac{1}{2}t - \log(N)}\right)^N. \end{aligned} \tag{36}$$

When $K \geq 2$, the CDF of T_{OSOMP} is summarized in Theorem 1.

Theorem 1. *In the case of $K \geq 2$, the CDF of T_{OSOMP} is given by*

$$F_{T_{\text{OSOMP}}}(t) = \omega_K \sum_{k=0}^{K-1} \frac{e^{-\left(\frac{kt}{2K}\right)}}{k!} \int_0^\infty q\left(y, \frac{t}{2}\right) r(y,k) y^{K-2} dy, \tag{37}$$

where

$$\omega_K = \frac{K^{K-1}}{(K-2)!}, \tag{38}$$

$$r(y,k) = e^{-y(K-k)}, \tag{39}$$

$$q\left(y, \frac{t}{2}\right) = e^{-e^{\left(y - \frac{t}{2K}\right)}}. \tag{40}$$

Proof. See Appendix C. □

Combining (36) and (37), we have (41) at the top of the following page.

$$F_{T_{\text{OSOMP}}}(t) = \begin{cases} \left(1-e^{-(\frac{t}{2}+\log(N))}\right)^N, & K=1, \\ \omega_K \sum_{i=0}^{K-1} \frac{e^{\left(-\frac{t}{2K}\right)}}{i!} \int_0^\infty q\left(y, \frac{t}{2}\right) r(y,i) y^{K-2} dy, & K \geq 2, \end{cases} \quad \text{Under } H_0. \tag{41}$$

It follows (41) that the P_{FA} is given by

$$\begin{aligned} P_{\text{FA}} &= P(T_{\text{OSOMP}} > \gamma | H_0) \\ &= 1 - F_{T_{\text{OSOMP}}}(\gamma), \end{aligned} \tag{42}$$

where γ represents the detection threshold. Based on the Neyman-Pearson criterion, γ can be calculated from (42) with a given $P_{\text{FA}} = \alpha$.

4.2. OSOMP Detector with Minimum Number of Iterations

As shown in Algoritm 1, the number of iterations is K. In practice, it is possible to use the first k ($k \leq K$) iterations to make a decision on whether the signal exists. To further reduce the amount of calculation, in this subsection, we discuss the minimum number of iterations k to achieve the desired detection probability and false alarm probability.

Algorithm 1 The Proposed OSOMP Detector

Input: $\boldsymbol{y}, \boldsymbol{\Psi}, \boldsymbol{\Psi}_{\text{c}}, \bar{\boldsymbol{\Phi}}, K, \sigma$ **Output**: Detection decision H_1/H_0

1. Initialize index set $\boldsymbol{\mu}_0 = \emptyset$, sensing matrix $\boldsymbol{\Theta} = \bar{\boldsymbol{\Phi}} P^{\perp}_{\boldsymbol{\Psi}_{\text{c}}} \boldsymbol{\Psi}$, and residual vector $\boldsymbol{r}_0 = \boldsymbol{y}$;
2. ***For*** $k = 1$ to $k = K$
3. Find the index μ_k as $\mu_k = \arg\max_{i \in \{1,\ldots,N\}} | < \mathbf{r}_{k-1}, \boldsymbol{\Theta}(i) > |$;
4. Update the support set $\boldsymbol{\mu}_k = \boldsymbol{\mu}_{k-1} \cup \{\mu_k\}$, and obtain the subspace $\hat{\boldsymbol{H}} = \boldsymbol{\Theta}(\boldsymbol{\mu}_k)$;
5. Calculate the projection operator $\mathbf{P}_{\hat{\boldsymbol{H}}} = \hat{\boldsymbol{H}} \left(\hat{\boldsymbol{H}}^H \hat{\boldsymbol{H}} \right)^{-1} \hat{\boldsymbol{H}}^H$;
6. Update the residual vector $\mathbf{r}_k = \left(\mathbf{I} - \mathbf{P}_{\hat{\boldsymbol{H}}} \right) \mathbf{y}$;
7. **End For**
8. Compute the equivalent test statistic $T_{\text{OSOMP}} = \frac{\sum_{k=1}^{K} \left\| \mathbf{P}_{\boldsymbol{\Theta}(\mu_k)} \left(\boldsymbol{\Phi}\boldsymbol{\Phi}^H \right)^{-\frac{1}{2}} \mathbf{y} \right\|_2^2}{\sigma^2/2} - 2K \log N$;
9. Obtain the detection threshold γ from (42) with a given probability of false alarm P_{FA};
10. **If** $T_{\text{OSOMP}} > \gamma$,
11. Output the decision H_1,
12. **else**
13. Output the decision H_0.
14. **End If**

Suppose that the desired $P_{\text{D}} = \tau_d$, $P_{\text{FA}} = \tau_f$, then, the minimum k is given by

$$\begin{aligned} &\min \quad k \\ &P_{\text{FA}} \leq \tau_f, \\ &P_{\text{D}} \geq \tau_d, \\ &1 \leq k \leq K. \end{aligned} \tag{43}$$

In radar detection, P_{FA} is an important parameter. According to the receiver operating characteristic, P_{D} decreases with P_{FA} [34]. Then, (43) can be rewritten as

$$\begin{aligned} &\min \quad k \\ &P_{\text{FA}} = \tau_f, \\ &T_k \geq \gamma_k, \\ &1 \leq k \leq K. \end{aligned} \tag{44}$$

where

$$T_k = \frac{\sum_{i=1}^{k} \left\| \mathbf{P}_{\boldsymbol{\Theta}(\mu_i)} \mathbf{C}^{-\frac{1}{2}} \mathbf{y} \right\|_2^2}{\sigma^2/2} - 2k \log N. \tag{45}$$

Based on the above analysis, the OSOMP detector with the minimum k is summarized in Algorithm 2. It is worth noting that (44) can also cope with the case of an unknown number of IOs.

Algorithm 2 OSOMP Detector with Minimum Number of Iterations k

Input: $\mathbf{y}, \boldsymbol{\Psi}, \boldsymbol{\Psi}_{\text{c}}, \bar{\boldsymbol{\Phi}}, K, \sigma$ **Output**: Detection decision H_1/H_0

1. Initialize index set $\boldsymbol{\mu}_0 = \emptyset$, sensing matrix $\boldsymbol{\Theta} = \bar{\boldsymbol{\Phi}} \mathbf{P}^{\perp}_{\boldsymbol{\Psi}_{\text{c}}} \boldsymbol{\Psi}$, and residual vector $\mathbf{r}_0 = \mathbf{y}$, $k = 1$;
2. Find the index μ_k as $\mu_k = \arg\max_{i \in \{1,\ldots,N\}} | < \mathbf{r}_{k-1}, \boldsymbol{\Theta}(i) > |$;
3. Update the support set $\boldsymbol{\mu}_k = \boldsymbol{\mu}_{k-1} \cup \{\mu_k\}$, and obtain the subspace $\hat{\boldsymbol{H}} = \boldsymbol{\Theta}(\boldsymbol{\mu}_k)$;
4. Calculate the projection operator $\mathbf{P}_{\hat{\boldsymbol{H}}} = \hat{\boldsymbol{H}} \left(\hat{\boldsymbol{H}}^H \hat{\boldsymbol{H}} \right)^{-1} \hat{\boldsymbol{H}}^H$;
5. Update the residual vector $\mathbf{r}_k = \left(\mathbf{I} - \mathbf{P}_{\hat{\boldsymbol{H}}} \right) \mathbf{y}$;
6. Compute the equivalent test statistic $T_k = \frac{\sum_{i=1}^{k} \left\| \mathbf{P}_{\boldsymbol{\Theta}(\mu_i)} \left(\boldsymbol{\Phi}\boldsymbol{\Phi}^H \right)^{-\frac{1}{2}} \mathbf{y} \right\|_2^2}{\sigma^2/2} - 2k \log N$;
7. Obtain the detection threshold γ_k from (42) with a given probability of false alarm $P_{\text{FA}} = \tau_f$;
8. **If** $T_k > \gamma_k$,
9. Output the decision H_1,
10. **break**
11. **else**
12. $k = k + 1$, go to step 2;
13. **If** $k > K$
14. Output the decision H_0.
15. **End If**
16. **End If**

5. Simulations

In this section, numerical simulations are conducted to verify the performance of the proposed detector. We assume that the transmitted signal $\mathbf{s}$ is a deterministic waveform while the noise $\mathbf{w}_{\text{sc}}$ is sampled from independent identically distributed complex Gaussian distribution with $\mathcal{CN}(\mathbf{0}, \sigma^2 \mathbf{I})$. Suppose the noise variance $\sigma^2 = 1$. From [14], the SNR is given by

$$\text{SNR} = 10 \log_{10} \frac{\frac{1}{KN} \sum_{k=1}^{K} \left(|\alpha_k|^2 \sum_{n=1}^{N} |s(n)|^2 \right)}{\sigma^2}. \tag{46}$$

We compare the proposed OSOMP detector with the CSD, which assumes full knowledge of the support, the cross correlation (CC) detector and the energy detector (ED) [14]. For consistency, we consider a compressive version of the CC detector, which is given by

$$T_{\text{CC}} = \frac{\sum_{k=1}^{K} |\mathbf{H}^H(k) \left(\boldsymbol{\Phi}\boldsymbol{\Phi}^H \right)^{-1} \mathbf{y}|^2}{\sigma^2} \underset{H_0}{\overset{H_1}{\gtrless}} \varsigma_{\text{CC}}, \tag{47}$$

where $\mathbf{H}^H(k)$ represents the k-th column of $\mathbf{H}$, and ς_{CC} denotes the detection threshold. Correspondingly, a compressive version of the ED is denoted as

$$T_{\text{ED}} = \frac{\left\| \left(\boldsymbol{\Phi}\boldsymbol{\Phi}^H \right)^{-\frac{1}{2}} \mathbf{y} \right\|_2^2}{\sigma^2/2} \underset{H_0}{\overset{H_1}{\gtrless}} \varsigma_{\text{ED}}, \tag{48}$$

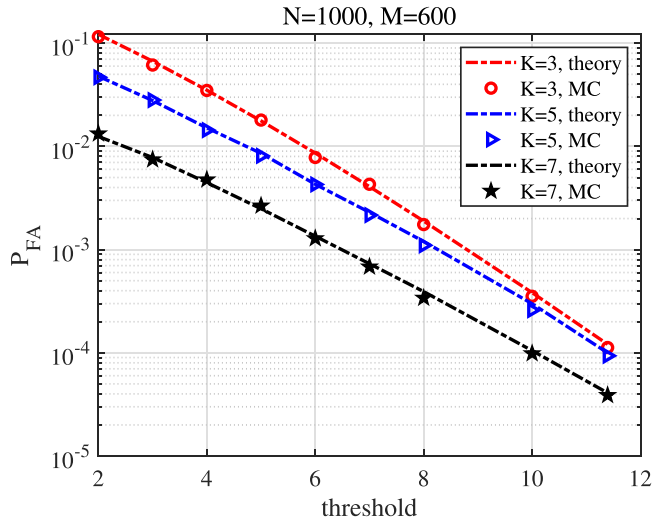

Fig. 4. P_{FA} of the OSOMP detector versus the detection threshold with different thresholds.

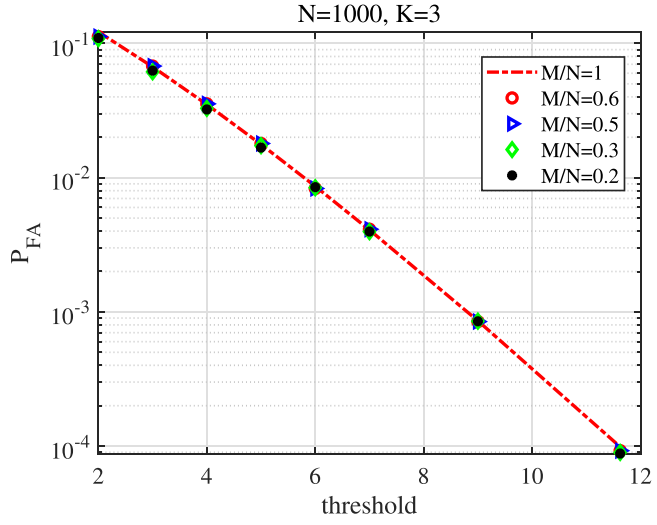

Fig. 5. P_{FA} versus the detection threshold with different compression ratios.

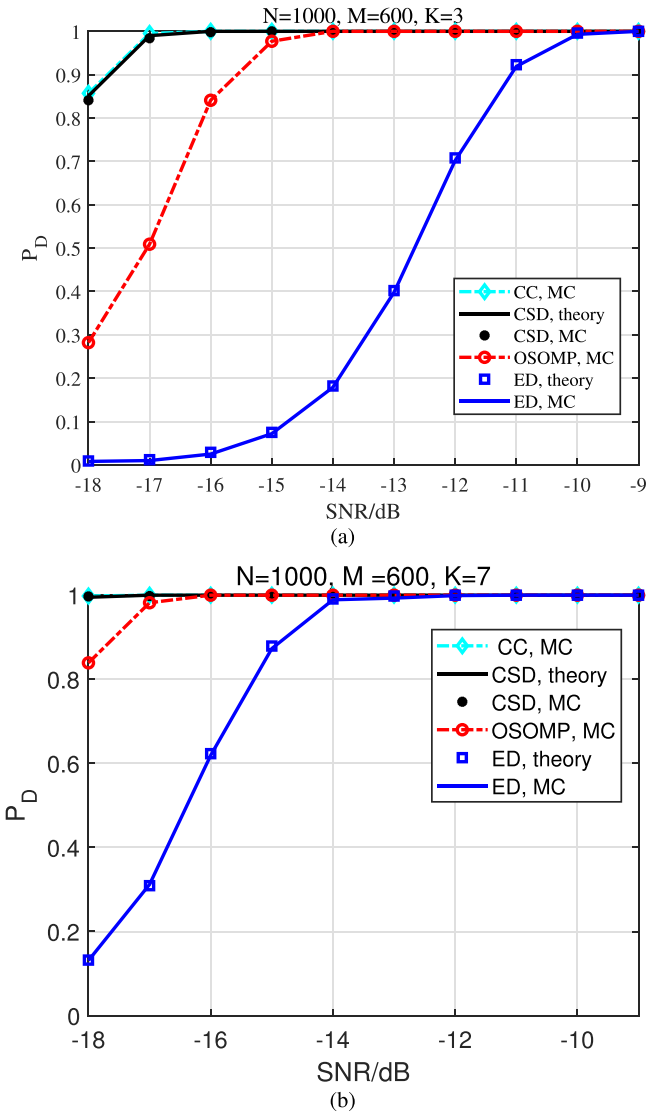

Fig. 6. Detection performance comparisons with $N = 1000$ for different SNRs. (a) $K = 3$; (b) $K = 7$.

where ς_{ED} is the detection threshold. The probability of false alarm P_{FA} and probability of detection P_{D} of the ED are given in Appendix D.

5.1. False Alarm of OSOMP

In the first experiment, we use Monte Carlo (MC) simulations to verify the expression of P_{FA} for the proposed OSOMP detector in (42) by varying the detection threshold with different numbers of IOs K. Specifically, we set $N = 1000$, $M = 600$, $L = 10$, $K \in \{3, 5, 7\}$, $\bar{\mathbf{\Phi}}$ is a Gaussian measurement matrix, and the dictionary matrix $\mathbf{\Psi}$ is obtained from (7)-(12). The number of MC simulations under each threshold is 100 divided by the probability of false alarm corresponding to the $y-$axis. As can be seen from Fig. 4, the MC curves match the theoretical ones well.

Fig. 5 shows that the P_{FA} of the OSOMP detector versus the detection threshold under different numbers of measurements, where we set $K = 3$, $N = 1000$, and $M \in \{1000, 600, 500, 300, 200\}$. It can be observed that when $M >> K$, the probability of false alarm has no difference with M, which can be observed from (41) that the P_{FA} only relates to K in the case of $K \geq 2$.

5.2. Detection Performance

We first compare the detection performance of the OSOMP detector (33) with the CSD (19), the CC detector (47) and the ED (48) under different SNRs. For this experiment, we select $K \in \{3, 7\}$, $N = 1000$, $M = 600$, time delay bins $Q = 40$, Doppler shift bins $2P + 1 = 25$, the range of Doppler $\Omega_p \in \{-0.48\pi : 0.04\pi : 0.48\pi\}$, $p = 1, \cdots, 2P + 1$, the number of interference $L = 10$, the dictionary basis matrix $\mathbf{\Psi}$ is built based on (7)-(12) and $P_{\text{FA}} = 10^{-4}$. The detection probability curves of these detectors are plotted in Fig. 6. The detection probability of the CSD and the ED are obtained by both theory and MC simulations, while the detection probability of OSOMP and CC detector are verified by MC simulations. The number of MC simulations under each SNR is 10^4. From Figs. 5 and 5, it can be observed that the CC detector as a banchmark performs the best, and CSD performs better than the OSOMP detector owing to that it requires the knowledge of the target support. When the support set is unknown, the proposed OSOMP detector outperforms the ED.

To offer details on the impact of the number of IOs, Fig. 7 depicts the probability of detection of the various detectors as a function of K, where we set $N = 1000$, $M = 600$, SNR $\in \{-18, -16\}$dB,

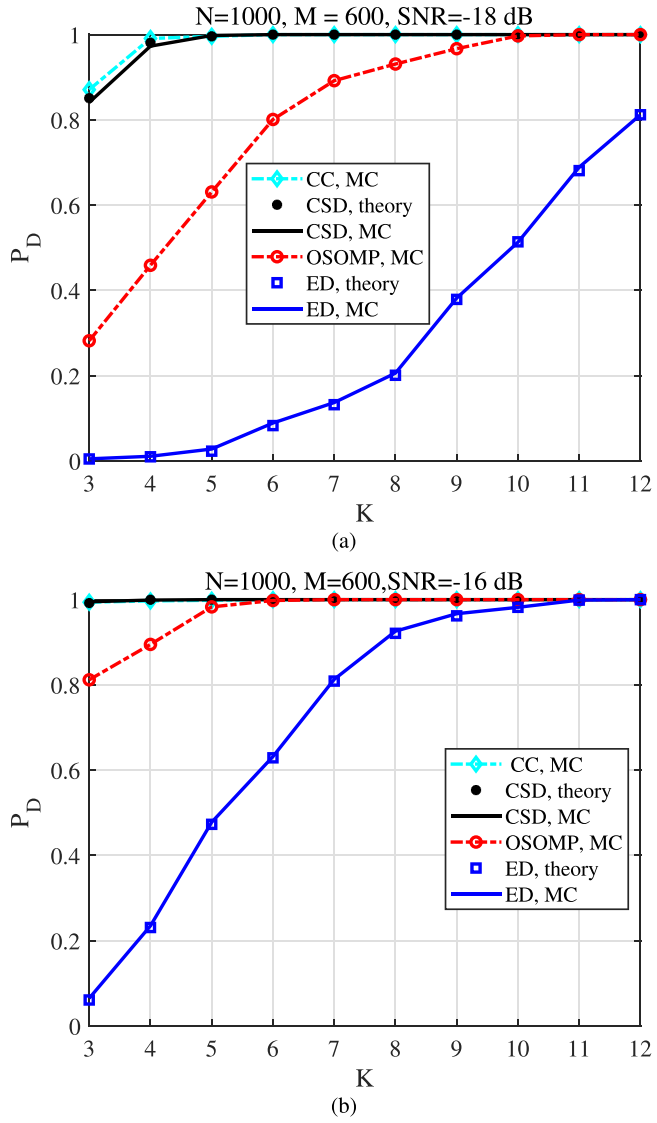

Fig. 7. Detection performance comparisons with $N = 1000$ for different K. (a) SNR=−18dB; (b) SNR=−16dB.

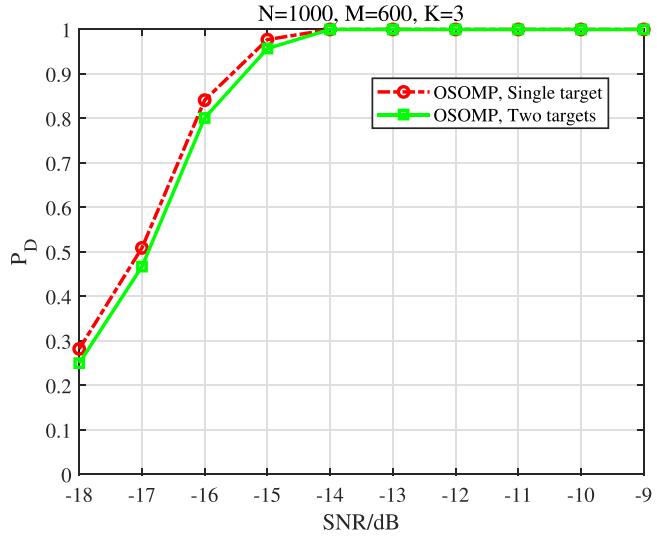

Fig. 8. OSOMP detector for multi-target detection.

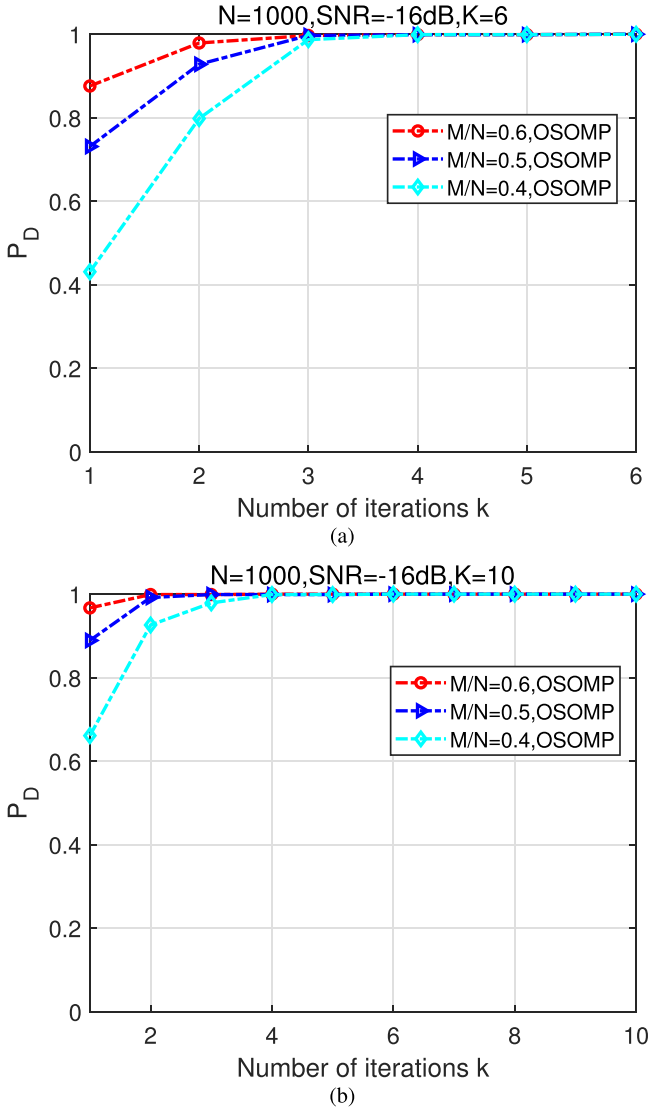

Fig. 9. OSOMP detector with different number of iterations. (a)$K = 6$; (b) $K = 10$.

and $P_{FA} = 10^{-4}$. It is seen that the detection performance improves with the increase of number of K, and the OSOMP detector always performs much better than the ED.

Fig. 8 illustrates that the OSOMP detector can be applied for multi-target detection. In this experiment, we set $M/N = 0.6$, $N = 1000$, $K = 3$, and we consider that there are a single target and two targets in the surveillance area, respectively. It is seen that compared with single target detection, multiple targets will reduce the performance of the OSOMP detector, because the target echoes outside the detection area are considered noise to increase the detection threshold setting.

Fig. 9 depicts the effect of detection performance of the OSOMP detector with the number of iterations. Here, we set $N = 1000$, $M/N \in \{0.4, 0.5, 0.6\}$, SNR= -16dB, $K \in \{6, 10\}$, the desired $\tau_f = 10^{-4}$, and $\tau_d = 0.975$. Fig. 9 (a) shows that when $K = 6$ and $M/N = 0.6$, two times of iterations can meet the desired conditions. Fig. 9 (b) shows that when $K = 10$ and $M/N = 0.4$, two times of iterations are enough to make a decision.

Fig. 10 shows the effect of the compression ratio on the detection performance of the various detectors under different SNRs, where $N = 1000$, $K = 3$, $M/N \in \{0.2,\ 0.25,\ 0.3,\ 0.4,\ 0.6,\ 1\}$, SNR $= -13$dB and $P_{FA} = 10^{-4}$. We see that the detection performance increases as the compression ratio increases. Specifically, when

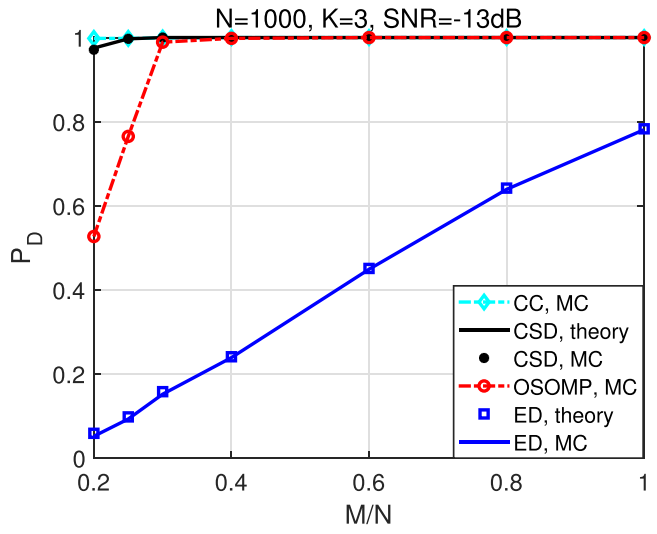

Fig. 10. Detection performance comparisons with $N = 1000$, $K = 3$ for different compression ratios.

$M/N = 0.3$, the probability of detection P_{D} of the OSOMP detector is 0.99, which matches that of the CC detector and CSD. On the other hand, the ED performs the worst in all compression ratios.

6. Conclusion

We studied the problem of target detection with DPI and clutter by using compressive observations in an SFN-based MS-PRS consisting of multiple IOs and one receiver. Due to the non-cooperative nature of the IOs, the position of the IOs may be inaccurately known in practical deployment. To address this problem, we first analyzed the CSD when the target support is known. For the case of unknown target support, an OSOMP detector was proposed by using OMP to estimate target support and projecting the compressive observations into the estimated subspace. As the OMP-induced order statistic is non-convergent in distribution, we proposed a modified and convergent test statistic for the OSOMP detector and provided an analytical expression for the probability of false alarm. To further reduce the amount of computation, we discussed how to determine the minimum number of iterations required to achieve the desired detection probability. Numerical simulations results demonstrate that the theoretical analysis of the probability of false alarm P_{FA} matches numerical simulations, and the performance of the OSOMP detector increases as the number of IOs increases. Besides, we also compared the detection performance under different number of targets and compression ratios. All MC simulation results show that in the case of unknown target support, the OSOMP detector outperforms the ED in low to moderate SNR regions.

Declaration of Competing Interest

We declare that we do not have any commercial or associative interest that represents a conflict of interest in connection with the work submitted.

CRediT authorship contribution statement

Junhu Ma: Methodology, Software, Writing – original draft. **Hongbin Li:** Methodology, Writing – review & editing. **Lu Gan:** Methodology, Writing – review & editing.

Data availability

Data will be made available on request.

Appendix A. Rank of $\boldsymbol{\Phi}\boldsymbol{\Phi}^{\boldsymbol{H}}$

It is observed from (13) that

$$\mathrm{rank}\left(\bar{\boldsymbol{\Phi}}\right) = M, \tag{A.1}$$

and

$$\mathrm{rank}\left(\mathbf{P}^{\perp}_{\boldsymbol{\Psi}_{\mathrm{c}}}\right) = N - L. \tag{A.2}$$

Assume that the basis of N dimensional $\boldsymbol{\Psi}$ is denoted as

$$\boldsymbol{\Psi} = \mathrm{span}(\boldsymbol{\kappa}_1, \ldots, \boldsymbol{\kappa}_N), \tag{A.3}$$

where vector $\boldsymbol{\kappa}_n \in \mathbb{C}^{N\times 1}$ represents the n-th column of $\boldsymbol{\Psi}$, and $\boldsymbol{\kappa}_m$, $\boldsymbol{\kappa}_n$ are independent each other for the case of $m \neq n$. The subspace of $\mathbf{s}_{\mathrm{c}}$ can be denoted as

$$\boldsymbol{\Psi}_{\mathrm{c}} = \mathrm{span}(\boldsymbol{\kappa}_1, \ldots, \boldsymbol{\kappa}_L), \tag{A.4}$$

and, we have

$$\mathbf{P}^{\perp}_{\boldsymbol{\Psi}_{\mathrm{c}}} = \mathrm{span}(\boldsymbol{\kappa}_{L+1}, \ldots, \boldsymbol{\kappa}_N). \tag{A.5}$$

Therefore, the rank of $\boldsymbol{\Phi}\boldsymbol{\Phi}^H$ is given by

$$\begin{aligned}&\mathrm{rank}\left(\boldsymbol{\Phi}\boldsymbol{\Phi}^H\right) = \mathrm{rank}\left(\bar{\boldsymbol{\Phi}}\mathbf{P}^{\perp}_{\boldsymbol{\Psi}_{\mathrm{c}}}\right)\\ &= \mathrm{rank}\left(\bar{\boldsymbol{\Phi}}\mathrm{span}(\boldsymbol{\kappa}_{L+1}, \ldots, \boldsymbol{\kappa}_N)\right)\\ &= \min\left(M, N-L\right).\end{aligned} \tag{A.6}$$

Due to $L \ll M \ll N$ and $N - L > M$, we have

$$\mathrm{rank}\left(\boldsymbol{\Phi}\boldsymbol{\Phi}^H\right) = M. \tag{A.7}$$

Appendix B. Analysis of the Complex-Valued CSD

Based on the distribution of T_{CSD}, the probability of false alarm P_{FA} of the CSD is

$$P_{\mathrm{FA}} = P(T_{\mathrm{CSD}} > \zeta_s | H_0) = \frac{\gamma\left(K, \frac{\zeta_s}{2}\right)}{\Gamma(K)}, \tag{B.1}$$

where $\frac{\gamma(a,x)}{\Gamma(K)}$ is the regularized Gamma function, $\Gamma(\cdot)$ denotes the Gamma function, $\gamma(a,x)$ is the lower Gamma function given by

$$\gamma(a,x) = \int_0^x t^{a-1}e^{-t}dt, \tag{B.2}$$

and ζ_s represents the detection threshold. The probability of detection (P_{D}) is given by

$$P_{\mathrm{D}} = P(T_{\mathrm{CSD}} > \zeta_s | H_1) = Q_K\left(\sqrt{\lambda_{\mathrm{CSD}}}, \sqrt{\zeta_s}\right), \tag{B.3}$$

where $Q_M(a,b)$ representing the Marcum Q function is expressed as

$$Q_K(a,b) = \int_b^{\infty} x\left(\frac{x}{a}\right)^{K-1} e^{-\frac{x^2+a^2}{2}} I_{K-1}(ax)dt, \tag{B.4}$$

with I_{K-1} denoting the modified Bessel function of first kind of order $K-1$ [34].

Appendix C. Proof of Theorem 1

Consider a standard exponential distribution given by

$$\bar{t}_i \sim \mathrm{Exp}(1) = e^{-t}, \quad i = 1, \ldots, N. \tag{C.1}$$

The order statistic of $\bar{t}_i$ is denoted as $\bar{t}_{(i)}$ satisfying

$$\bar{t}_{(1)} \leq \cdots \leq \bar{t}_{(i)} \leq \cdots \leq \bar{t}_{(N)}, \tag{C.2}$$

and the trimmed sums of $\bar{t}_{(i)}$ [33] is denoted as

$$\bar{T}_K = \sum_{i=N-K+1}^{N} \bar{t}_{(i)} - K\log(N). \tag{C.3}$$

Lemma 1. When $K \geq 2$, and N is sufficiently large, the CDF $F_{\bar{T}_K}(t)$ of $\bar{T}_K$ converges to

$$\begin{aligned} F_{\bar{T}_K}(t) &= P\left(F_{\bar{T}_K}(t) \leq t\right) \\ &= \omega_K \sum_{k=0}^{K-1} \frac{e^{(-(kt/K))}}{k!} \int_0^\infty q(y,t) r(y,k) y^{K-2} dy, \end{aligned} \tag{C.4}$$

where

$$q(y,t) = e^{-e^{\left(y-\frac{t}{K}\right)}}, \tag{C.5}$$

ω_K and $r(y,k)$ are defined in (38) and (39), respectively.

Proof: See [33,35].

Combining (33) and (C.3), we have

$$T_{\text{OSOMP}} = 2\bar{T}_K. \tag{C.6}$$

Based on Lemma 1, the CDF $F_{T_{\text{OSOMP}}}(t)$ is given by

$$\begin{aligned} F_{T_{\text{OSOMP}}}(t) &= P(T_{\text{OSOMP}} \leq t) \\ &= P\left(\bar{T}_K \leq \tfrac{t}{2}\right) = F_{\bar{T}_K}\left(\tfrac{t}{2}\right) \\ &= \omega_K \sum_{k=0}^{K-1} \frac{e^{-\left(\frac{kt}{2K}\right)}}{k!} \int_0^\infty q\left(y, \tfrac{t}{2}\right) r(y,k) y^{K-2} dy, \end{aligned} \tag{C.7}$$

where $\omega_K = \frac{K^{K-1}}{(K-2)!}$, $q\left(y, \frac{t}{2}\right) = e^{-e^{\left(y-\frac{t}{2K}\right)}}$, and $r(y,k) = e^{-y(K-k)}$, which closes the proof.

Appendix D. Performance of the ED

From (15) and (17), we have

$$\begin{cases} \mathbf{y} \sim \mathcal{CN}\left(\mathbf{0}, \sigma^2 \bar{\mathbf{\Phi}} \mathbf{P}^{\perp}_{\mathbf{\Psi}_c} \bar{\mathbf{\Phi}}^H\right), & \text{under } H_0, \\ \mathbf{y} \sim \mathcal{CN}\left(\mathbf{\Theta}\boldsymbol{\alpha}, \sigma^2 \bar{\mathbf{\Phi}} \mathbf{P}^{\perp}_{\mathbf{\Psi}_c} \bar{\mathbf{\Phi}}^H\right), & \text{under } H_1. \end{cases} \tag{D.1}$$

Then, the distribution of T_{ED} is

$$\begin{cases} T_{\text{ED}} = \dfrac{\left\| \left(\bar{\mathbf{\Phi}} \mathbf{P}^{\perp}_{\mathbf{\Psi}_c} \bar{\mathbf{\Phi}}^H\right)^{-\frac{1}{2}} \mathbf{y} \right\|_2^2}{\sigma^2/2} \sim \chi^2_{2M}, & \text{under } H_0, \\ T_{\text{ED}} = \dfrac{\left\| \left(\bar{\mathbf{\Phi}} \mathbf{P}^{\perp}_{\mathbf{\Psi}_c} \bar{\mathbf{\Phi}}^H\right)^{-\frac{1}{2}} \mathbf{y} \right\|_2^2}{\sigma^2/2} \sim \chi^2_{2M}(\lambda_{\text{ED}}), & \text{under } H_1, \end{cases} \tag{D.2}$$

where $\left(\bar{\mathbf{\Phi}} \mathbf{P}^{\perp}_{\mathbf{\Psi}_c} \bar{\mathbf{\Phi}}^H\right)^{-\frac{1}{2}}$ represents the whitening operator, and $\lambda_{\text{ED}} = \dfrac{\left\| \left(\bar{\mathbf{\Phi}} \mathbf{P}^{\perp}_{\mathbf{\Psi}_c} \bar{\mathbf{\Phi}}^H\right)^{-\frac{1}{2}} \mathbf{\Theta}\boldsymbol{\alpha} \right\|_2^2}{\sigma^2/2}$. Based on (B.1) and (B.3), the probability of false alarm P_{FA} of the ED is given by

$$P_{\text{FA}} = \frac{\gamma\left(M, \frac{\varsigma_{\text{ED}}}{2}\right)}{\Gamma(M)}, \tag{D.3}$$

where ς_{ED} denotes the detection threshold. The probability of detection P_{D} of the ED is expressed as

$$P_{\text{D}} = Q_M\left(\sqrt{\lambda_{\text{ED}}}, \sqrt{\varsigma_{\text{ED}}}\right), \tag{D.4}$$

where the expression of the Marcum Q function is expressed in (B.4).

References

[1] H.D. Griffiths, C.J. Baker, An introduction to passive radar, Artech House, 2017.
[2] M. Edrich, A. Schroeder, Multiband multistatic passive radar system for airspace surveillance: A step towards mature PCL implementations, in: Proc. IEEE Int. Conf. Radar, 2013, pp. 218–223.
[3] S. Gogineni, M. Rangaswamy, B.D. Rigling, A. Nehorai, Ambiguity function analysis for UMTS-based passive multistatic radar, IEEE Trans. Signal Process. 62 (11) (2014) 2945–2957.
[4] G. Battistelli, L. Chisci, S. Morrocchi, F. Papi, A. Farina, A. Graziano, Robust multisensor multitarget tracker with application to passive multistatic radar tracking, IEEE Trans. Aerosp. Electron. Syst. 48 (4) (2012) 3450–3472.
[5] J.H.G. Ender, On compressive sensing applied to radar, Signal Process. 90 (5) (2010) 1402–1414.
[6] K.S. Bialkowski, I.V.L. Clarkson, Passive radar signal processing in single frequency networks, in: Proc. 46th Asilomar Conf. Signals, Syst. Comput. (ASILOMAR), 2012, pp. 199–202.
[7] M. Malanowski, Detection and parameter estimation of manoeuvring targets with passive bistatic radar, IET Radar, Sonar Navig. 6 (8) (2012) 739–745.
[8] X. Zhang, H. Li, B. Himed, Multistatic detection for passive radar with direct-path interference, IEEE Trans. Aerosp. Electron. Syst. 53 (2) (2017) 915–925.
[9] G. Fabrizio, F. Colone, P. Lombardo, A. Farina, Adaptive beamforming for high-frequency over-the-horizon passive radar, IET Radar, Sonar, Navig. 3 (4) (2009) 384–405.
[10] D.K.P. Tan, H. Sun, Y. Lu, M. Lesturgie, H.L. Chan, Passive radar using global system for mobile communication signal: theory, implementation and measurements, Proc. Inst. Electr. Eng. - Radar, Sonar Navig. 152 (3) (2005) 116–123.
[11] F. Colone, D.W. O'Hagan, P. Lombardo, C.J. Baker, A multistage processing algorithm for disturbance removal and target detection in passive bistatic radar, IEEE Trans. Aerosp. Electron. Syst. 45 (2) (2009) 698–722.
[12] Y. Liu, J. Yi, X. Wan, X. Zhang, H. Ke, Evaluation of clutter suppression in CP-OFDM-based passive radar, IEEE Sensors J. 19 (14) (2019) 5572–5586.
[13] K.S. Bialkowski, I.V.L. Clarkson, S.D. Howard, Generalized canonical correlation for passive multistatic radar detection, in: Proc. IEEE Statist. Signal Process. Workshop (SSP), 2011, pp. 417–420.
[14] J. Liu, H. Li, B. Himed, Two target detection algorithms for passive multistatic radar, IEEE Trans. Signal Process. 62 (22) (2014) 5930–5939.
[15] B.K. Chalise, B. Himed, GLRT detector in single frequency multi-static passive radar systems, Signal Process. 142 (2018) 504–512.
[16] H. Zhao, J. Liu, Z. Zhang, H. Liu, S. Zhou, Linear fusion for target detection in passive multistatic radar, Signal Process. 130 (2017) 175–182.
[17] M. Radmard, S.M. Karbasi, M.M. Nayebi, Data fusion in MIMO DVB-T-Based passive coherent location, IEEE Trans. Aerosp. Electron. Syst. 49 (3) (2013) 1725–1737, doi:10.1109/TAES.2013.6558015.
[18] P. Wang, J. Fang, N. Han, H. Li, Multiantenna-assisted spectrum sensing for cognitive radio, IEEE Transactions on Vehicular Technology 59 (4) (2010) 1791–1800.
[19] P. Maechler, N. Felber, H. Kaeslin, Compressive sensing for WiFi-based passive bistatic radar, in: Proc. 20th Eur. Signal Process. Conf., 2012, pp. 1444–1448 .
[20] M. Weiß, Compressive sensing for passive surveillance radar using DAB signals, in: IEEE Int. Radar Conf., 2014, pp. 1–6.
[21] M.N. Tabassum, M.A. Hadi, S. Alshebeili, CS based processing for high resolution GSM passive bistatic radar, in: Proc. IEEE Int. Conf. Acoust., Speech, Signal Process. (ICASSP), 2016, pp. 2229–2233.
[22] X. Zhang, J. Swärd, H. Li, A. Jakobsson, B. Himed, A sparsity-based passive multistatic detector, IEEE Trans. Aerosp. Electron. Syst. 55 (6) (2019) 3658–3666.
[23] W. Qiu, E. Giusti, A. Bacci, M. Martorella, F. Berizzi, H. Zhao, Q. Fu, Compressive sensingbased algorithm for passive bistatic isar with DVB-T signals, IEEE Trans. Aerosp. Electron. Syst. 51 (3) (2015) 2166–2180.
[24] W. Feng, J. Friedt, G. Cherniak, M. Sato, Batch compressive sensing for passive radar range-doppler map generation, IEEE Trans. Aerosp. Electron. Syst. 55 (6) (2019) 3090–3102.
[25] L. Anitori, M. Otten, W. van Rossum, A. Maleki, R. Baraniuk, Compressive CFAR radar detection, in: Proc. IEEE Radar Conf., 2012, pp. 0320–0325.
[26] M.A. Davenport, P.T. Boufounos, M.B. Wakin, R.G. Baraniuk, Signal processing with compressive measurements, IEEE J. Sel. Topics Signal Process. 4 (2) (2010) 445–460.
[27] J. Ma, L. Gan, H. Liao, I. Zahid, Sparse signal detection without reconstruction based on compressive sensing, Signal Process. 162 (2019) 211–220.
[28] A. Hariri, M. Babaie-Zadeh, Joint compressive single target detection and parameter estimation in radar without signal reconstruction, IET Radar, Sonar Navig. 9 (8) (2015) 948–955.
[29] A. Razavi, M. Valkama, D. Cabric, Compressive detection of random subspace signals, IEEE Trans. Signal Process. 64 (16) (2016) 4166–4179.
[30] T. Wimalajeewa, P.K. Varshney, Sparse signal detection with compressive measurements via partial support set estimation, IEEE Trans. Signal Inf. Process. Netw. 3 (1) (2017) 46–60.
[31] J.A. Tropp, A.C. Gilbert, Signal recovery from random measurements via orthogonal matching pursuit, IEEE Trans. Inf. Theory 53 (12) (2007) 4655–4666.
[32] O. Mahfoudia, F. Horlin, X. Neyt, Performance analysis of the reference signal reconstruction for DVB-T passive radars, Signal Process. 158 (2019) 26–35.
[33] N. Balakrishnan, E.C. Ron, J.M.S. Alegría, Advances in Distribution Theory, Order Statistics, and Inference, birkhäuser, 2006.
[34] S. Kay, Fundamentals of Statistical Signal Processing: Detection Theory, Prentice-Hall, 1993.
[35] H.N. Nagaraja, Some nondegenerate limit laws for the selection differential, Ann. Statist. (1982) 1306–1310.